Probing the structural and electronic properties of zirconium doped boron clusters: Zr distorted B12 ligand framework

Probing the structural and electronic properties of zirconium doped boron clusters: Zr distorted B_{12} ligand framework

Weiguo Sun[a,b], Xinxin Xia[b], Cheng Lu[*a,c], Xiaoyu Kuang[*b], Andreas Hermann[*d]

[a]*Department of Physics, Nanyang Normal University, Nanyang 473061, China*

[b]*Institute of Atomic and Molecular Physics, Sichuan University, Chengdu 610065, China*

[c]*Department of Physics and High Pressure Science and Engineering Center, University of Nevada, Las Vegas, Nevada 89154, United States*

[d]*Centre for Science at Extreme Conditions and SUPA, School of Physics and Astronomy, The University of Edinburgh, EdinburghEH9 3JZ, United Kingdom*

Abstract

As an extension of boron based materials, transition-metal (TM) doped boron clusters deserve interest in controlling size-dependent structural and electronic properties. Herein, using Crystal structure AnaLYsis by Particle Swarm Optimization (CALYPSO) method and density functional theory (DFT) calculations, we have performed a global search for the lowest-energy structures of ZrB_n^Q (n= 10-20, Q= 0, -1) clusters with n= 10-20. The results show that the ground-state structures of the obtained clusters feature a distinctive structural evolution pattern, from half-sandwich bowls to distorted drum-like and then to Zr-centered distorted tubular motifs. For the sake of validity of current ground-state structures, photoelectron spectra (PES) are predicted from time-dependent DFT calculations. More interestingly, the neutral and anionic ZrB_{12} clusters are found to possess enhanced stability in the size regime studied here. The stability of closed shell half-sandwich ZrB_{12} cluster is analyzed by intrinsic bond orbitals (IBO) and Adaptive Natural Density Partitioning (AdNDP) method, which indicates that the stability mechanism is caused by dopant Zr atom breaking the boron bowl's triangle B_3 unit to form a quasi-linear B_3 unit in B_{12} and enhance both the interaction of the B-B σ-bonds and the Zr-B π-bonds.

1 Introduction

The structural and electronic properties of atomic and molecular clusters have received considerable attention in physics and material science due, in part, to they constitute intermediate phases between individual atom and bulk solid [1,2]. They can be used to understand how the fundamental properties of materials evolve from isolated atoms or small molecules to a bulk phase [2,3]. Recent efforts have been made toward making boron-based nanowires, nanotubes and nanosheets, which potentially have structures resembling assemblies of smaller boron clusters [3-5]. A series of 2D boron-based structures and borophenes extend the richness of boron clusters [6-10], where the combination of σ-type and π-type bonds may result in the planarity of the species. PES experiments and quantum chemistry calculations have unveiled the most stable structures on their respective potential energy surface [4,5,7-10], which imply a large variety of novel building blocks to add to the known rich chemistry of size-selected boron clusters. The smallest doubly aromatic isomer, the triangular B_3^- species, possesses localized B-B bonds as well as delocalized π- and σ-bonds that make it the most stable structure [11]. Meanwhile, cationic B_3^+ is, due to π-aromaticity, an effective inorganic ligand allowing complexation with CO and N_2, both of which have been characterized by infrared spectroscopy [12,13].

The C_{6v} symmetry anionic B_7^- cluster is akin to the B_3 isomers, i.e. doubly aromatic, while unique umbrella-type structures of AlB_7^- and AlB_8^- are based on the enhanced stability of the quasi-planar B_7^- wheels [14,15]. More recently, the lanthanide elements Pr which has very low electronegativity, forms a half-sandwich structure together with a B_7^{3-} ligand [16]. Larger perfectly planar molecular wheels with a high coordination number of the central boron atom (B_8^-, B_9^-, B_8^{2-} ...) have been suggested as new inorganic ligands, and as robust and stable assembly building blocks [17,18]. Subsequently, the molecular wheel M@B_8 and M@B_9 species have been synthesised, where M represents quite different doping atoms, such as the C, Al, and transition metals [14, 19-22]. The striking highly stable aromatic quasi-planar B_{12} and its corresponding anionic species possess a bowl structure, with a nine-membered outer ring and a B_3 triangle inner ring, and forms the basis for the C_{3v} half-sandwich

$M@B_{12}^-$ (M = Co, Rh, Ir) structures [23, 24]. Moreover, suitably doped metal centers supported by the B_{12}^- bowl structure can further bind with small molecules (CO, CO_2 and N_2) with high bond activation. Saha *et al*. tested $M@B_{12}^-$ (M = Co, Rh, Ir) clusters in chemical reactions with CO and N_2 as promising adsorbent candidates [25], which inspired searches for other reported appropriate metal bound boron ligands to bind various small molecules with strong bond activation [26]. In addition, more complex boron-based ligands (B_{16}^-, B_{18}^- ...) have been reported in recent years, which lead to searches for novel nano-systems with tunable electronic, optical and other interesting properties [27-30].

The transition metal zirconium is chemical very resistive, and is mainly used as a refractor and an opacifier [31]. Solid dodecaboride ZrB_{12} is a superconductor, where covalent interactions in the B_{12} cages may cause the dynamic stabilities and good mechanical properties promoting Zr-driven superconductivity [32-35]. Therefore, if boron clusters are able to house doped Zr atom to form stable systems, these novel building blocks could be used to manipulate various physicochemical properties of boron-based materials. This encouraged us to perform an extensive study on Zr-doped boron clusters, which by themselves could serve as new ligands to capture small gas molecules or become reaction centers and model catalysts [25, 26]. Consequently, we have carried out unbiased structure searches to identify the most stable structures on the potential energy surfaces of differently charged zirconium doped boron clusters in the size range of n= 10-20 by the CALYPSO method. The simulated PES coupled with DFT calculations serve as an effective approach to obtain detailed information about the structure of predicted ZrB_n clusters. We have also calculated the corresponding electronic properties and deciphered stabilization mechanism of the special clusters.

2 Computation Details

In order to determine the low-lying isomers of ZrB_n clusters, we have performed separate structure searches for neutral and anionic clusters for the size range of n= 10-20, using the particle swarm optimization (PSO) algorithm for cluster structure prediction [35] as implemented in CALYPSO code, details of which can be found

elsewhere [36-37]. Briefly, the high search efficiency is achieved by several techniques included in the PSO algorithm, e.g. point group symmetry constraints on structural generation (a random choice from C_1 to C_6) and utilizing bond characterization matrices (BCM) for the elimination of similar structures [35]. The validity of the CALYPAO method has been demonstrated in successful applications ranging from clusters to crystal structure predictions [38-45].

In our structure searches, each generation contains 50 structures, 80% of which are produced by the PSO algorithm, whereas 20% are new and generated randomly. As the cluster size increases, determination of true global minima becomes increasingly challenging because of the much increased complexity of the potential surface and the exponential increase of the number of local minima. High-level *ab initio* calculations with a large basis set should be required in the structure search to determine the true global minimum. However, with current computer facilities, high-level *ab initio* calculations with very large basis sets are still impractical for medium-sized clusters beyond n= 16. Here, we have adopted a compromise method in two stages. Firstly, we performed the expensive global structure searches at (PBE0/Zr/LanL2DZ/B/6-31G) level of theory. We followed at least 20-30 generations in the CALYPSO cluster structure search, depending on cluster size, to generate at least 1000-1500 structurally different low-lying isomers for each cluster size. Searches were rerun independently at each cluster size to ensure the global minimum was indeed found reliably, while non-converged searches were extended until no new low-energy candidates appeared in the final stages of the search. Subsequently, among the 1000-1500 isomers, the top 50 low-lying isomers with energy difference from the lowest-energy isomers less than 3 eV are collected as candidates for determination the lowest-energy structures, and further re-optimized at (PBE0/Zr/def2-TZVP/B/6-311+G(d)) level to identify the true global minimum structure at each cluster size.

All the energetically low-lying structures are fully relaxed without geometry and spin constrains until the forces are smaller than a criterion of convergence. The DFT calculations are carried out by using the generalized gradient exchange-correlation hybrid Perdew-Burke-Ernzerhof (PBE0) [46] as implemented in in the Gaussian 09

suite [47]. The all electron basis set 6-311+G(d) [48] is used for the B atom and def2-TZVP [49] for the Zr atom. Multiple spin states and vibrational frequency calculation are all considered in the process of the refined structure re-optimizations. In order to test the reliability of our calculations, we have calculated the neutral Zr_2, B_2 and ZrB_2 dimers through many different functionals (HF [50], B3LYP [51], PW91 [52], PBE [53], B3PW91 [54] as well as CCSD(T) [55]) with 6-311+G(d) and def2-TZVP basis sets for B and Zr atom, respectively. The calculated results are summarized in Table S1. From there, it is found that the bond lengths R and vibrational frequencies ω of the three molecules obtained with the PBE0 functional are in good agreement with the available experimental values [56,57,58]. So, PBE0/Zr/def2-TZVP/B/6-311+G(d) has been selected as a reasonable method for ZrB_n clusters. The same level of theory, PBE0/Zr/def2-TZVP/B/6-311+G(d), has also been used for DFT calculations of TM Co doped boron clusters [59].

Moreover, we have also simulated the photoelectron spectra of the anionic ZrB_n clusters using time-dependent density functional theory (TD-DFT) method. The IBO [60,61] and AdNDP [62] bonding analyses are performed using the Multiwfn [63] program package to gain further insight into the bonding mechanisms present in these clusters.

3 Results and Discussion

3.1 Geometric Structures and Photoelectron Spectra

Based on the systematic detailed search of the potential energy surfaces by the CALYPSO method and combined with the re-optimized refined DFT calculations, the lowest-energy structures of neutral and anionic ZrB_n clusters were obtained in the size range of $10 \leqslant n \leqslant 20$. The lowest-energy structures of ZrB_n^Q (n = 10-20, Q = 0, -1) clusters along with their point group symmetries are displayed in Figure 1. The most relevant metastable structures for each size are shown in Figure S1 in the Supporting Information. More information about the lowest-energy structures of ZrB_n^Q (n = 10-20, Q = 0, -1) clusters is collected in Table S2.

Generally speaking, as shown in Figure 1, the geometric structures can differ

drastically from pure boron clusters when TM zirconium is present for doping [64]. Pure boron clusters are characterized by planar or quasi-planar structure in their ground states, while the ZrB_n exhibit 3D structures for all clusters sizes up to n = 20. For neutral ZrB_n clusters, distinct half-sandwich structures emerge at n = 10, 11, with Zr centered inside the boron bowls and slightly out of plane of their quasi-planar structures. In the ZrB_{12} cluster, the Zr atom adopts a vertex within the bowl structure, which otherwise features a nine membered outer boron ring and an inner quasi-linear B_3 unit that is slightly out of plane. For larger size-selected clusters, ZrB_{13} can be seen as adding two B atoms to the center of the ZrB_{11} cluster. For $14 \leqslant n \leqslant 19$, except for n = 15, the clusters form distorted drum-like structures comprising two boron rings sandwiching the Zr atom, with point group symmetries C_s or C_{2v} (all displayed in Figure 1). For the ZrB_{15} species, the Zr atom is centered in a bowl-like B ring structure with four-membered inner rings akin to similar boron half-sandwich structures that bind to other transition metals [24, 25]. The neutral ZrB_{20} cluster possess a tubular structure with two additional B atom bridging atop the distorted B_{18} drum. This structure lies 0.36 eV lower in energy than the perfect D_{2d} drum-like structure.

For the anionic species, an obvious structural evolution pattern shows that Zr doped boron clusters evolve from a half-sandwich structure (n = 10) to distorted double ring structures at n = 14, and then to distorted Zr centered drum-like structures for n = 20. For n = 10-13, the TM Zr atom is out of the plane of the B_n circular ring, and ZrB_{12}^- possesses a transitional half-sandwich structure, which is formed by a quasi-linear B_3 unit combined with nine outer-ring B atoms. Prior works have shown that B_{12}^- would be the best ligand candidate to form novel C_{3v} half-sandwich coordination complexes with TMs [23, 24] due to the C_s symmetry of the B_{12}^- structures [50]. This is different to the C_s-symmetric ZrB_{12}^- we have obtained. The reason for this may be that the Zr atom is too small to stabilize the bare C_s symmetry of the B_{12}^- ring [65] compared with the $M@B_{12}^-$ (M = Co, Rh, Ir) clusters [23, 24]. With the B atom number increasing from 14 through 18, distorted drum-like anionic ZrB_n^- clusters exhibit a Zr

atom in the center of boron double rings, the latter possibly not fully closed. The global minimum of ZrB_{19}^- is cage-like of C_s symmetry, and can be seen as two B atoms capping a Zr-centered distorted drum-like structure. Similar to the reported TaB_{20}^- structure [66], the lowest-energy ZrB_{20}^- species obtained by CALYPSO is also characterized by a Zr atom caged in tubular molecular motif C_s symmetry with a B_2 species bridging the drum B_{18} structure. This structure is found to be more stable by 0.26 eV than the ideal double-ringed alternative.

To confirm the ground-state structures of the ZrB_n^- clusters, the photoelectron spectra of the anionic ZrB_n clusters are simulated by TD-DFT method [67,68]. Regarding the ZrB_n^- PES calculations, the first band represents the detachment transition from the ground state of ZrB_n^- to that of neutral ZrB_n clusters, and thus gives the vertical detachment energy (VDE). The calculated VDE as well as the adiabatic detachment energy (ADE) obtained by the corresponding intersection between the baseline and the rising edge of the first peak are collected in Table S3. As shown in Figure 2, a large number of bands occurs in the spectra for n = 10, 11 in the binding energy range 1.5 eV to 5.0 eV. The VDE of ZrB_{10}^- is lower than that of ZrB_{11}^- due to the different geometric structure, however they otherwise possess very similar spectral patterns. For the ZrB_{12}^- species, a busy spectrum emerges for 2.9-4.5 eV, while the VDE the ZrB_{12}^- cluster lies about 1.0 eV lower in binding energy than that of $M@B_{12}^-$ (M = Co, Rh, Ir) [23, 24]. The crucial reason for this difference may be related to the smaller size of dopant Zr compared to the group-9 atoms, which also manifests itself in a different geometric structure. For ZrB_n^- with n = 13-18, all the PES bands have relatively similar pattern, with distinctive peaks in the binding energy range of about 2.50-3.60 eV. More continuous peaks are seen for binding energies in the range 3.60-5.00 eV. For the ZrB_{19}^- cluster, a large VDE value of 3.57 eV is seen, accompanied by two obvious shoulders at higher energies. The ZrB_{20}^- cluster features major prominent peaks in the binding energy range 2.61-5.00 eV. Its first peak is located at 2.62 eV, which is lower than in the ZrB_{19}^- species, and may be due to the distortion of the Zr-centered drum-like structure in this cluster. Based on previously seen robust analyses of computed and experimental PES data, we believe that the

predicted theoretical spectra will stimulate follow-up computational and experimental investigations in the Zr-doped boron clusters system.

3.2 Relative Stabilities of ZrB_n^Q (n = 10-20, Q = 0, -1) Clusters

To estimate the relative stability of the re-optimized lowest-energy ZrB_n^Q (n = 10-20, Q = 0, -1) clusters, the binding energy per atom (E_b) and second energy difference (Δ^2E) are shown in Figure 3, defined by the following formulae:

$$E_b(ZrB_n^Q) = [(n)E(B) + E(Zr^Q) - E(ZrB_n^Q)]/n+1, Q = 0, -1$$

$$\Delta^2 E(ZrB_n^Q) = E(ZrB_{n-1}^Q) + E(ZrB_{n+1}^Q) - 2E(ZrB_n^Q), Q = 0, -1.$$

The E_b represents the energy gain of adding a neutral or anionic Zr atom to an assembly of boron atoms, and exhibits a gradual monotonic growth as a function of the number of B atoms (Figure 3a). Clearly, the anionic clusters have higher values than corresponding neutral species and imply enhanced stability. And with the cluster size increasing, the values $E_b(n)$ for both the neutral and anionic ZrB_n clusters gradually flatten out with increased n, indicating that successively larger clusters are relatively stable. Another sensitive physical parameter Δ^2E helps characterize relative stability of certain clusters against neighboring smaller or larger clusters, and is shown in Figure 3b. For the neutral ZrB_n isomers, an apparent odd-even oscillation appears, with distinct peaks located at even sizes, which indicates that the ZrB_n with n = 12, 14, 16… and closed shell electronic structures are more stable than the respective adjacent clusters. For the corresponding anionic species, the stabilities are also reflected by the Δ^2E alternation. The Zr doped B_{12} clusters, both neutral and anionic species, exhibit high stability compared to their neighbors, presumably due to stable distorted half-sandwich structure of the ZrB_{12} isomer.

A large energy difference between the highest occupied molecular orbital and lowest unoccupied molecular orbital (HOMO-LUMO gap), also labeled by E_{gap}, implies high kinetic stability and low chemical reactivity, as it would be unfavorable to accept electrons into a high-lying unoccupied molecular orbital, or to donate electrons from a low-lying occupied molecular orbital [69]. On this basis, the E_{gap} values of neutral and anionic ZrB_n clusters are listed in Table 1 and the cluster size

dependence of E_{gap} is shown in Figure 3c. Comparing the E_{gap} of cluster in both charge states, the noticeable peaks for ZrB_{12} and ZrB_{12}^- imply their enhanced relative stability, a tendency that is parallel to the analysis of Δ^2E. The neutral clusters' E_{gap} values for even-sized clusters are mostly higher than for odd-sized clusters because the numbers of valence electrons are paired and thus possess closed-shell structures, while for the anionic ZrB_n clusters, we can see a less clear dependency on boron atom number, and the most stable structure can be ascribed to ZrB_{12}^- with the local maximum E_{gap}= 2.78 eV.

3.3 The Localized Molecular Orbital and Chemical Bonding Analyses of ZrB_{12} Cluster

The Zr doping of B clusters may have enormous effects on geometry and electronic behavior. The analysis described in the previous section implies special enhanced stability and chemically inert species for ZrB_{12} and ZrB_{12}^- cluster because the Zr dopant broke the B_{12} unit geometry. The relative stabilities analysis indicated that the ZrB_{12} cluster with closed shell valence electronic has a large HOMO-LUMO gap about 2.83 eV. Further elucidation should come from intrinsic bond orbital (IBO) analysis of the neutral ZrB_{12} localized molecular orbitals (LMOs), shown in Figure 4.

For better understanding the high stability of neutral ZrB_{12} cluster, the bonding patterns have been analyzed by IBO [60]. The IBO method is based on maximizing a certain localization functional for unitarily transformed MO's, which can provide a direct connection between quantum chemistry and intuitive chemical concepts [61]. For simplicity, we have performed the IBO calculations and show selected occupied LMOs of the neutral ZrB_{12} cluster in Figure 4, while the corresponding IBOs of the ZrB_{12}^- cluster are given in Figure S2. From these graphics, we can see distinctly the B-B bonds in the peripheral B_9 ring interact with the central doped Zr atom, which manifests in multicenter σ bonding LMOs. The 4*d*-type atomic orbital of the doped Zr atom also features, and the linear B_3 unit also interacts with the Zr atom to form a σ bond. Analysing the LMOs in the neutral ZrB_{12} cluster system, the IBOs of the peripheral B_9 ring structure and the linear B_3 unit are strongly localized on B-B-Zr LMOs. This suggests that σ bonding is the root cause for the highly stable species.

The bonding nature of the interactions between the Zr and B atoms in the neutral ZrB_{12} cluster were further elucidated by the AdNDP method and presented in Figure 5 (the corresponding AdNDP bonding pattern of ZrB_{12}^- cluster are depicted in Figure S3). AdNDP is an extension of natural bond orbital analysis [62]. There are eleven delocalized 3c-2e σ-bonds among the peripheral B and Zr atoms. Nine of these 3c-2e σ-bonds could be ascribed to the interactions in triangular B-B-B units among the B_{12} species (ON = 1.920-1.971 |e|), while another two sets of 3c-2e σ-bonds feature in the quasi-linear B_3 unit (ON = 1.890 |e|). One 4c-2e bond is involved in the σ-bond between the *d*-type AO of the Zr and *p*-type AO of B atoms, the ON = 1.954 |e| of which, instead of the ideal 2.00 |e|, indicates the partial covalent bonding in this system. There are four more delocalized bonds, two pairs of 5c-2e σ-bonds and two pairs of 7c-2e π-bonds patterns. The first two 5c-2e σ-bonds characterize the interaction along the outside of the peripheral B atoms, with ON = 1.963 |e|, while another pair of 5c-2e σ-bonds describe the interaction of Zr with five peripheral B atoms. The already discussed inclination to form delocalized π-bonds between the dopant Zr atom and the centered linear B_3 unit emerges again in two pairs of 7c-2e bonds with different ON, 1.927 and 1.890 |e|, respectively. The 7c-2e π-bonds are responsible for the bonding between the *d*-type AO Zr atom and *p*-type B atoms in the linear B_3 unit, while some σ-bonds amongst peripheral B atoms could also be observed. It is worth to pointing out that the ZrB_{12} clusters contain σ-bonds mainly due to the B-B interactions, especially the σ-bonds in linear B_3 unit and the peripheral B_9 ring, and π-bonds that rely on the *d*-type AO Zr atom, which make it overall a particularly stable species.

4 Conclusion

Through an analysis of ZrB_n^Q (n = 10-20, Q = 0, -1) clusters by the combination of CALYPSO and DFT methodology, the ground-state structures of the proposed clusters are characterized by a distinctive structural evolution pattern, from the half-sandwich structure to distorted drum-like structures and then to Zr-centered distorted tubular motifs. We expect that the predictive theoretical PES data will stimulate follow-up computational and experimental investigations of the ZrB_n cluster

system. Meanwhile, according to analysis of the relative stabilities, the neutral and anionic ZrB_{12} clusters are found to have special enhanced stability among the size range of n = 10-20. The stability of the lowest-energy structure ZrB_{12} is analyzed by IBO and AdNDP methods, which show that the dopant Zr atom breaks the triangle B_3 to form a quasi-linear B_3 unit in B_{12} motif and induce strong Zr-B interactions that enhance the stability of the neutral half-sandwich ZrB_{12} cluster.

ACKNOWLEDGMENTS

This work was supported by the National Natural Science Foundation of China (Nos. 11574220, 11304167, and 21671114), the Special Program for Applied Research on Super Computation of the NSFC-Guangdong Joint Fund (the second phase) under Grant No. U1501501, and the Program for Science & Technology Innovation Talents in Universities of Henan Province (No. 15HASTIT020). Parts of the calculations were performed using the Cherry Creek Supercomputer in National Supercomputing Institute of the UNLV.

References:

1. H.-J. Zhai, B. Kiran, J. Li and L.-S. Wang, *Nat. Mater.*, 2003, **2**, 827–833.
2. J. Tian, Z. Xu, C. Shen, F. Liu, N. Xu and H. J. Gao, *Nanoscale* 2010, **2**, 1375−1389.
3. X. Fu and J. Yuan, *Nanoscale* 2013, **5**, 9067−9072.
4. R . B. Patel, T. Chou and Z. Iqbal, *J. Nanomater*. 2015, **16**, 14.
5. H.-S. Piazza, Zachary A.and Hu, W.-L. Li, Y.-F. Zhao, J. Li and L.-S. Wang, *Nat. Commun.*, 2014, **5**, 3113.
6. A. J. Mannix, X.-F. Zhou, B. Kiraly, J. D. Wood, D. Alducin, B. D. Myers, X. Liu, B. L. Fisher, U. Santiago, J. R. Guest, M. J. Yacaman, A. Ponce, A. R. Oganov, M. C. Hersam and N. P. Guisinger, *Science*, 2015, **350**, 1513–1516.
7. Li, Wei-Li, Chen, Qiang, Tian, Wen-Juan, Bai, Hui, Zhao, Ya-Fan, Hu, Han-Shi, Li, Jun, Zhai, Hua-Jin, Li, Si-Dian and Wang Lai-Sheng. *J. Am. Chem. Soc.*, 2014, 136, 12257-12260.
8. H. R. Jiang, Z. H. Lu, M. C. Wu, F. Ciucci, T. S. Zhao. *Nano Energy*, 2016, **23**, 97-104.
9. Q. Chen, W.-L. Li, Y.-F. Zhao, S.-Y. Zhang, H.-S. Hu, H. Bai, H.-R. Li, W.-J. Tian, H.-G. Lu, H.-J. Zhai, S.-D. Li, J. Li and L.-S. Wang, *ACS Nano*, 2015, **9**, 754–760.
10. H.-J. Zhai, Y.-F. Zhao, W.-L. Li, Q. Chen, H. Bai, H.-S. Hu, Z. A. Piazza, W.-J. Tian, H.-G. Lu, Y.-B. Wu, Y.-W. Mu, G.-F. Wei, Z.P. Liu, J. Li, S.-D. Li and L.-S. Wang, *Nat. Chem.*, 2014, **6**, 727–731.
11. Zhai, H. J., Wang, L. S., Alexandrova, A. N., Boldyrev, A. I., Zakrzewski, V. G, *J. Phys. Chem. A* 2003, **107**, 9319 – 9328.
12. Zubarev D Y and Boldyrev A I., *J. Comput. Chem.* 2007, **28**, 251-268.
13. Jin, J., Wang, G., Zhou, M., Andrada, D. M., Hermann, M. and Frenking, G., *Angew. Chem. Int. Ed.*, 2016, **55**, 2078-2082.
14. Romanescu, C., Sergeeva, A. P., Li, W. L., Boldyrev, A. I. and Wang, L. S. *J. Am. Chem. Soc.*, 2011, **133**, 8646-8653.
15. Alexandrova, A. N., Boldyrev, A. I., Zhai, H. J.and Wang, L. S., *J. Phys. Chem. A*, 2004, **108**, 3509-3517.
16. Chen, T. T., Li, W. L., Jian, T., Chen, X., Li, J. and Wang, L. S., *Angew. Chem. Int. Ed*., 2017, **56**, 6916–6920.
17. H.-J. Zhai, A. N. Alexandrova, K. A. Birch, A. I. Boldyrev and L.-S. Wang, *Angew. Chem., Int. Ed.*, 2003, **42**, 6004-6008.
18. A. N. Alexandrova, H.-J. Zhai, L.-S. Wang and A. I. Boldyrev, *Inorg. Chem.*, 2004, **43**, 3552–3554.
19. C. Romanescu, T. R. Galeev, W.-L. Li, A. I. Boldyrev and L.-S. Wang, *J. Chem. Phys.*, 2013, 138, 134315.
20. W.-L. Li, C. Romanescu, T. R. Galeev, Z. A. Piazza, A. I. Boldyrev and L.-S. Wang, *J. Am. Chem. Soc.*, 2012, **134**, 165–168.
21. C. Romanescu, T. R. Galeev, W.-L. Li, A. I. Boldyrev and L.-S. Wang, *Angew. Chem., Int. Ed.*, 2011, 50, 9334–93378.

22. Averkiev, B. B., Wang, L. M., Huang, W., Wang, L. S., & Boldyrev, A. I. *Phys. Chem. Chem. Phys.*, 2009, **11**, 9840–9849
23. I. A. Popov, W.-L. Li, Z. A. Piazza, A. I. Boldyrev and L.-S. Wang, *J. Phys. Chem. A*, 2014, **118**, 8098–8105.
24. Liu, L., Moreno, D., Osorio, E., Castro, A. C., Pan, S., Chattaraj, P. K, T. Heine and G. Merino, *RSC Adv.*, 2016, **6**, 27177-27182.
25. Saha, R., Kar, S. and Pan, S., *J. Phys. Chem. A*, 2017, **121**, 2971−2979.
26. Wang, W., Zhang, X., Li, P., Sun, Q., Li, Z., Ren, C. and Guo, C. *J. Phys. Chem. A*, 2015, **119**, 796−805.
27. Moreno, D., Pan, S., Zeonjuk, L. L., Islas, R., Osorio, E., Martínez-Guajardo, G. and Merino, G. *Chem. Commun.*, 2014, **50**, 8140-8143.
28. Jiménez‐Halla, J. O. C., Islas, R., Heine, T. and Merino, G. *Angew. Chem. Int. Ed.*, 2010, 49(33): 5668-5671.
29. Huang, W., Sergeeva, A. P., Zhai, H. J., Averkiev, B. B., Wang, L. S. and Boldyrev, A. I., *Nat. Chem.*, 2010, **2**, 202-206.
30. Sergeeva, A. P., Averkiev, B. B., Zhai, H. J., Boldyrev, A. I. and Wang, L. S., *J. Chem. Phys.*, 2011, **134**, 224304.
31. Fu, X., Li, J., Luo, Z., Chen, X. and Ning, C., *J. Chem. Phys.*, 2017, **147**, 064306.
32. Gasparov, V. A., Sheikin, I., Levy, F., Teyssier, J. and Santi, G., *Phys. Rev. Lett.*, 2008, **101**, 097006.
33. Teyssier, J., Lortz, R., Petrovic, A., Van Der Marel, D., Filippov, V. and Shitsevalova, N., *Phys. Rev. B*, 2008, **78**, 134504.
34. Teyssier, J., Kuzmenko, A. B., Van Der Marel, D., Marsiglio, F., Liashchenko, A. B., Shitsevalova, N. and Filippov, V., *Phys. Rev. B*, 2007, **75**, 134503.
35. J. Lv, Y.-C. Wang, L. Zhu and Y.-M. Ma, *J. Chem. Phys.*, 2012, **137**, 084104.
36. Y.-C. Wang, J. Lv, L. Zhu and Y.-M. Ma, *Phys. Rev. B*, 2010, **82**, 094116.
37. Y.-C. Wang, J. Lv, L. Zhu and Y.-M. Ma, *Comput. Phys. Commun.*, 2012, **183**, 2063 – 2070.
38. L. Zhu, H.-Y. Liu, C. J. Pickard, G.-T. Zou and Y.-M. Ma, *Nature Chem.*, 2014, **6**, 644–648.
39. Y.-W. Li, J. Hao, H.-Y. Liu, Y.-L. Li and Y.-M. Ma, *J. Chem. Phys.*, 2014, **140**, 174712.
40. H. Wang, J. S. Tse, K. Tanaka, T. Iitaka and Y.-M. Ma, *Proc. Natl. Acad. Sci. USA*, 2012, **109**, 6463–6466.
41. J. Lv, Y.-C. Wang, L. Zhu and Y.-M. Ma, *Phys. Rev. Lett.*, 2011, **106**, 015503.
42. L. Zhu, H. Wang, Y.-C. Wang, J. Lv, Y.-M. Ma, Q.-L. Cui, Y.-M. Ma and G.-T. Zou, *Phys. Rev. Lett.*, 2011, **106**, 145501.
43. C. Lu, Q. Li, Y. Ma and C. F. Chen, *Phys. Rev. Lett.* 2017, **119**,115503.
44. C. Lu, M. Miao and Y. Ma, *J. Am. Chem. Soc.* 2013, **135**, 14167−14171.
45. V. N. Robinson, Y. Wang, Y. Ma and A. Hermann, *Proc. Natl. Acad. Sci. USA* 2017, **114**, 9003−9008.
46. Adamo, C.; Barone, V., *J. Chem. Phys.*, 1999, **110**, 6158-6170.
47. M. J. Frisch, G. W. Trucks, H. B. Schlegel, G. E. Scuseria, M. A. Robb, J. R. Cheeseman, J. A. Montgomery, Jr, T. Vreven, K. Kudin, J. Burant, J. M. Millam, S.

S. Iyengar, J. Tomasi, V. Barone, B. Mennucci, M. Cossi, G. Scalmani, N. Rega, G. A. Petersson, H. Nakatsuji, M. Hada, M. Ehara, K. Toyota, R. Fukuda, J. Hasegawa, M. Ishida, T. Nakajima, Y. Honda, O. Kitao, H. Nakai, M. Klene, X. Li, J. E. Knox, H. P. Hratchian, J. B. Cross, V. Bakken, C. Adamo, J. Jaramillo, R. Gomperts, R. E. Stratmann, O. Yazyev, A. J. Austin, R. Cammi, C. Pomelli, J. Ochterski, P. Y. Ayala, K. Morokuma, P. S. G. A. Voth, J. J. Dannenberg, V. G. Zakrzewski, S. Dapprich, A. D. Daniels, M. C. Strain, O. Farkas, D. K. Malick, A. D. Rabuck, K. Raghavachari, J. V. O. J. B. Foresman, Q. Cui, A. G. Baboul, S. Clifford, J. Cioslowski, B. B. Stefanov, G. Liu, A. Liashenko, P. Piskorz, R. L. M. I. Komaromi, D. J. Fox, T. Keith, M. A. Al-Laham, C. Y. Peng, A. Nanayakkara, M. Challacombe, P. M. W. Gill, B. G. Johnson, W. Chen, M. W. Wong, C. Gonzalez and J. A. Pople, Gaussian 09, revision C.0, Gaussian, Inc., Wallingford, CT, 2009.

48. A. D. McLean and G. S. Chandler, *J. Chem. Phys.*, 1980, **72**, 5639-5648.
49. Weigend, F. and Ahlrichs, R., *Phys. Chem. Chem. Phys.*, 2005, **7**, 3297-3305.
50. Cheeseman, J. R., Trucks, G. W., Keith, T. A. and Frisch, M. J. *J. Chem. Phys.* 1996, **104**, 5497–5509.
51. Becke, A. D. *J. Chem. Phys.* 1993, **98**, 5648–5652.
52. Perdew, J. P. and Wang, Y. *Phys. Rev. B* 1992, **45**, 13244–13249.
53. Perdew, J. P., Burke, K. and Ernzerhof, M. *Phys. Rev. Lett.* 1996, 77, 3865–3868.
54. Perdew, J. P., Ziesche, P. and Eschrig, H. Electronic Structure of Solids, ed. Akademie Verlag, Berlin, **1991**.
55. Barlett, R. J. and Musia, M. *Rev. Mod. Phys.* 2007, 79, 291–352.
56. K. P. Huber, and G. Herzberg, Molecular Spectra and Molecular Structure, Vol. 4. Constants of Diatomic Molecules (*Van Nostrand Reinhold*, New York, 1979).
57. J. R. Lombardi and B. Davis. *Chem. Rev.* 2002, **102**, 2431.
58. J. G. Yao, X. W. Wang and Y. X. Wang, *Chem. Phys.* 2008, **351**, 1-6.
59. Popov, I. A.; Jian, T.; Lopez, G. V.; Boldyrev, A. I. and Wang, L. S. *Nat. Commun.* 2015, **6**, 8654.
60. G. Knizia, *J. Chem. Theory Comput.* 2013, **9**, 4834−4843.
61. G. Knizia, J. E. Klein, *Angew. Chem. Int. Ed.* 2015, **54**, 5518−5522.
62. D. Y. Zubarev and A. I. Boldyrev, *Phys. Chem. Chem. Phys.*, 2008, **10**, 5207–5217.
63. Lu, T. and Chen, F., *Eur. Phys. J. D*, 2011, **106**, 043401.
64. L.-S. Wang, *Int. Rev. Phys. Chem.*, 2016, **35**, 69–142.
65. W.-L. Li, C. Romanescu, Z. A. Piazza and L.-S. Wang, *Phys. Chem. Chem. Phys.*, 2012, **14**, 13663–13669.
66. W.-L. Li, T. Jian, X. Chen, H.-R. Li, T.-T. Chen, X.-M. Luo, S.-D. Li, J. Li and L.-S. Wang, *Chem. Commun.*, 2017, **53**, 1587–1590.
67. Sun, W. G., Wang, J. J., Lu, C., Xia, X. X., Kuang, X. Y. and Hermann, A., *Inorg. Chem.*, 2017, **56**, 1241-1248.
68. Li, P., Sun, G., Bai, J., Wang, W., Bao, G. and Lu, C., *New J. Chem.*, 2017, **41**, 11208-11214.
69. Gao, Y., Bulusu, S.and Zeng, X. C., *J. Am. Chem. Soc.*, 2005, **127**, 15680-15681.

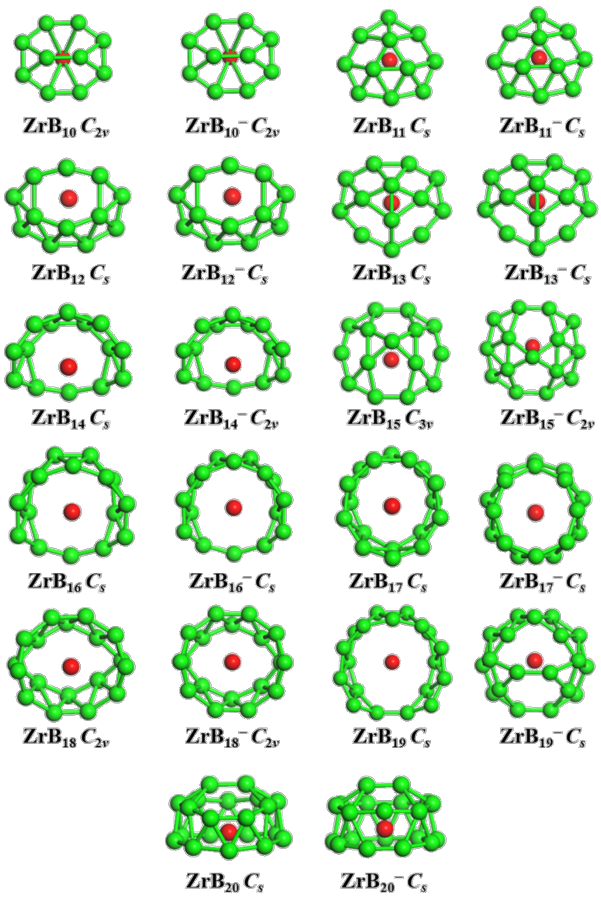

Figure 1. Lowest-energy structures of ZrB_n^Q (n = 10-20, Q = 0, -1) clusters along with their point group symmetries.

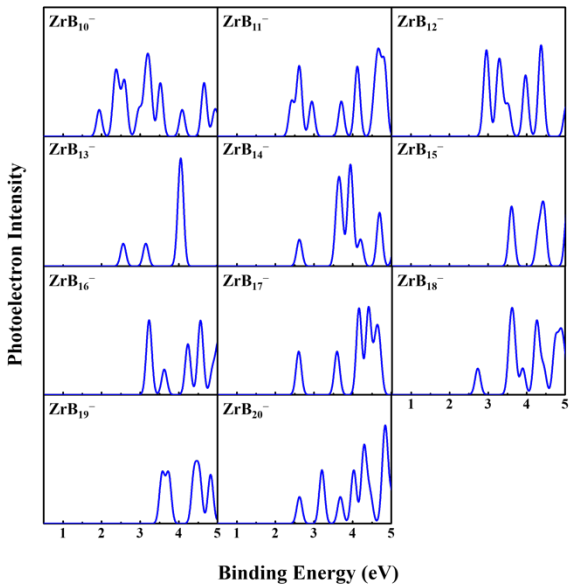

Figure 2. The simulated photoelectron spectra of anionic ZrB_n^- (n = 10-20) clusters.

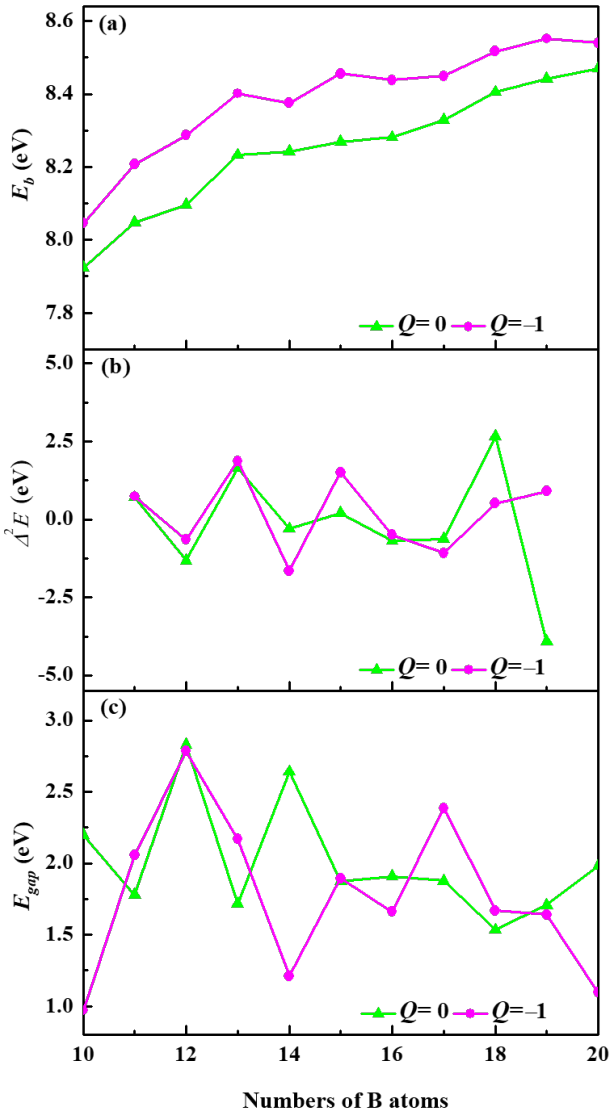

Figure 3. The binding energy per atom (E_b), second energy difference ($\Delta^2 E$) and the HOMO–LUMO gap (E_{gap}) for the lowest-energy neutral and anionic ZrB_n^Q (n = 10-20, Q = 0, -1) clusters.

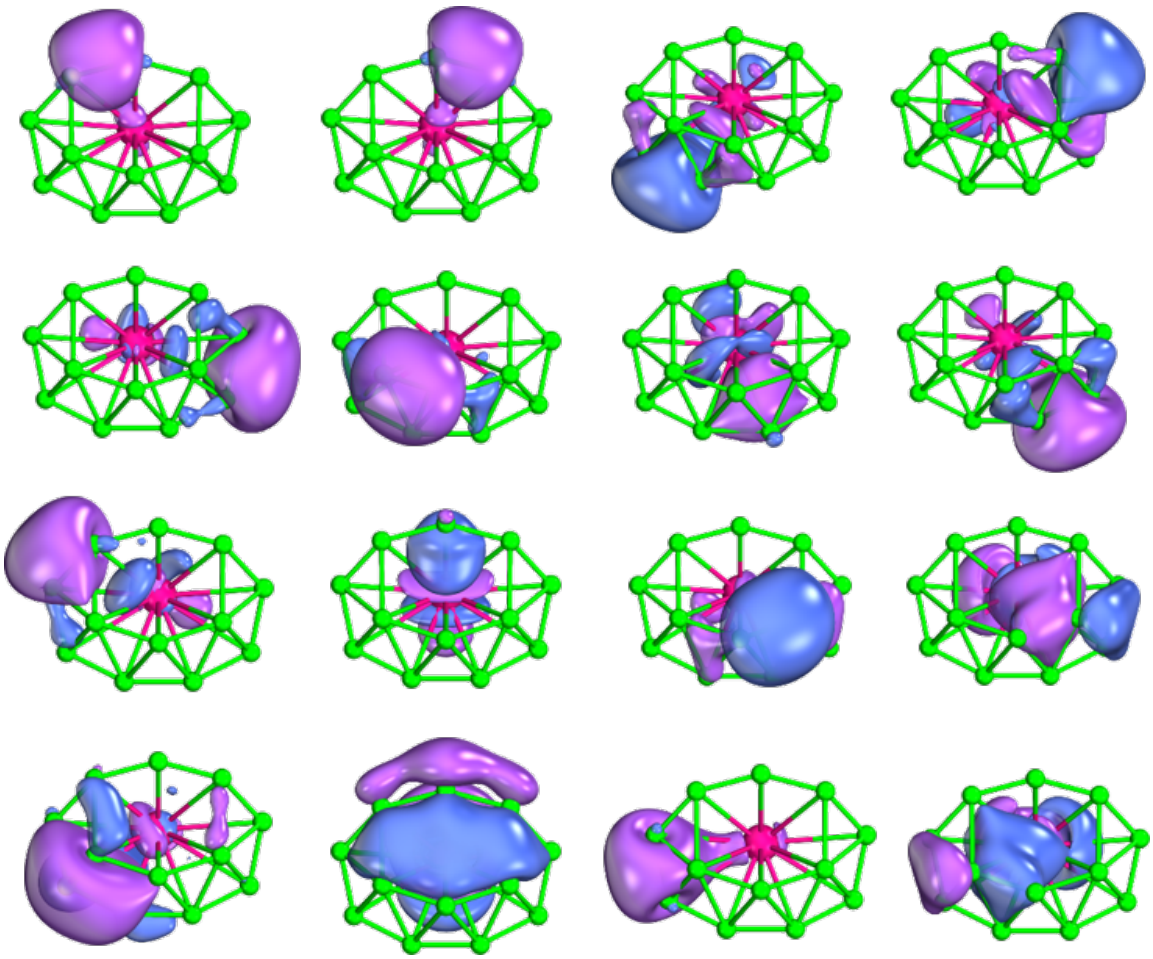

Figure 4. The intrinsic bond orbitals of neutral ZrB_{12} cluster visualized by IboView [61]. The iso-surfaces enclose 80% of the orbital's electron density.

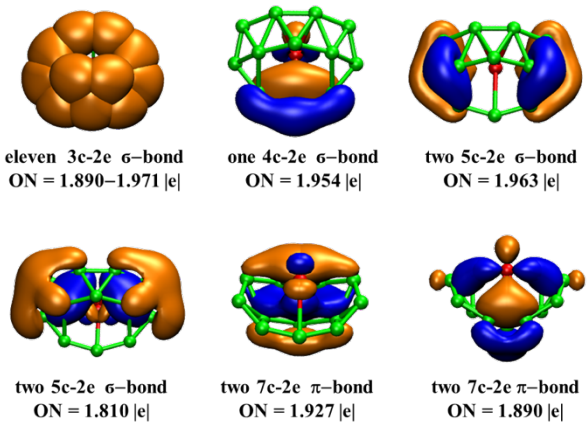

Figure 5. AdNDP bonding pattern of neutral ZrB_{12} cluster. ON stands for occupation number.